HAL
open science

# Loss of the actin-like protein MamK has pleiotropic effects on magnetosome formation and chain assembly in Magnetospirillum gryphiswaldense

Emanuel Katzmann, André Scheffel, Manuela Gruska, Jürgen M Plitzko, Dirk Schüler

## To cite this version:

Emanuel Katzmann, André Scheffel, Manuela Gruska, Jürgen M Plitzko, Dirk Schüler. Loss of the actin-like protein MamK has pleiotropic effects on magnetosome formation and chain assembly in Magnetospirillum gryphiswaldense. Molecular Microbiology, 2010, 10.1111/j.1365-2958.2010.07202.x . hal-00552637

**HAL Id: hal-00552637**

**https://hal.science/hal-00552637v1**

Submitted on 6 Jan 2011

**HAL** is a multi-disciplinary open access archive for the deposit and dissemination of scientific research documents, whether they are published or not. The documents may come from teaching and research institutions in France or abroad, or from public or private research centers.

L'archive ouverte pluridisciplinaire **HAL**, est destinée au dépôt et à la diffusion de documents scientifiques de niveau recherche, publiés ou non, émanant des établissements d'enseignement et de recherche français ou étrangers, des laboratoires publics ou privés.

molecular microbiology

# Loss of the actin-like protein MamK has pleiotropic effects on magnetosome formation and chain assembly in *Magnetospirillum gryphiswaldense*

| | |
|---|---|
| Journal: | *Molecular Microbiology* |
| Manuscript ID: | MMI-2010-09908.R1 |
| Manuscript Type: | Research Article |
| Date Submitted by the Author: | 29-Apr-2010 |
| Complete List of Authors: | Katzmann, Emanuel; Ludwig-Maximilians-Universität München, Biologie 1, Mikrobiologie; Max Planck Institut für Biochemie, Molekulare Strukturbiologie<br>Scheffel, André; Georgia Institute of Technology, School of Chemistry and Biochemistry<br>Gruska, Manuela; Max Planck Institute für Biochemie, Molekulare Strukturbiologie<br>Plitzko, Jürgen; Max Planck Institute für Biochemie, Molekulare Strukturbiologie<br>Schüler, Dirk; Ludwig-Maximilians-Universität München, Biologie 1, Mikrobiologie |
| Key Words: | MamK, cytoskeleton, actin-like, magnetotactic, cryo-electron tomography |
| | |

scholarONE™
Manuscript Central

# Loss of the actin-like protein MamK has pleiotropic effects on magnetosome formation and chain assembly in *Magnetospirillum gryphiswaldense*

Emanuel Katzmann[1,2], André Scheffel[3=], Manuela Gruska[2], Jürgen M. Plitzko[2], Dirk Schüler[1*]

Email: emanuel.katzmann@bio.lmu.de, gruska@biochem.mpg.de, plitzko@biochem.mpg.de

*Corresponding author

Telephone: +49 89 21 80 - 74502

Fax: +49 89 21 80 - 74515

Email: dirk.schueler@lmu.de

Keywords: MamK, cytoskeleton, actin-like, magnetotactic, cryo-electron tomography, organelles

[1]Ludwig-Maximillians-Universität München, Department Biologie I, Bereich Mikrobiologie, Biozentrum der LMU, D-82152 Martinsried, Germany

[2] Max Planck Institute of Biochemistry, Department of Molecular Structural Biology, Am Klopferspitz 18,

D-82152 Martinsried, Germany

[3] Max Planck Institute for Marine Microbiology, Celsiusstr.1, D-28359 Bremen, Germany

[=] Present address: School of Chemistry and Biochemistry, Georgia Institute of Technology, Atlanta, GA 30332–0400, USA.

Email: ascheffel3@mail.gatech.edu

For Peer Review

## Summary

Magnetotactic bacteria synthesize magnetosomes, which are unique organelles consisting of membrane-enclosed magnetite crystals. For magnetic orientation individual magnetosome particles are assembled into well-organized chains. The actin-like MamK and the acidic MamJ proteins were previously implicated in chain assembly. While MamK was suggested to form magnetosome-associated cytoskeletal filaments, MamJ is assumed to attach the magnetosome vesicles to these structures. Although the deletion of either *mamK* in *M. magneticum*, or *mamJ* in *M. gryphiswaldense* affected chain formation, the previously observed phenotypes were not fully consistent, suggesting different mechanisms of magnetosome chain assembly in both organisms. Here we show that in *M. gryphiswaldense* MamK is not absolutely required for chain formation. Straight chains, shorter, fragmented, and ectopic, were still formed in a *mamK* deletion mutant, although magnetosome filaments were absent as shown by cryo-electron tomography. Loss of MamK also resulted in reduced numbers of magnetite crystals and magnetosome vesicles and led to the mislocalization of MamJ. In addition, extensive analysis of wildtype and mutant cells revealed previously unidentified ultrastructural characteristics in *M. gryphiswaldense*. Our results suggest that, despite of their functional equivalence, loss of MamK proteins in different bacteria may result in distinct phenotypes, which might be due to a species-specific genetic context.


For Peer Review

## Introduction

The ability of magnetic navigation in magnetotactic bacteria (MTB) is based on the synthesis of magnetosomes, which are complex intracellular organelles. In *Magnetospirillum gryphiswaldense* MSR-1 (in the following referred to as MSR) and related magnetospirilla magnetosomes comprise cubo-octahedral nanocrystals of magnetite ($Fe_3O_4$) that are enveloped by vesicles of the magnetosome membrane (MM) (Gorby *et al.*, 1988; Schüler, 2004b). Previous studies revealed that the MM is a phospholipid bilayer, which is associated with a set of about 20 specific proteins (Gorby *et al.*, 1988; Grünberg *et al.*, 2001; Grünberg *et al.*, 2004). In *M. magneticum* AMB-1 (in the following referred to as AMB) it was shown that the MM originates via invagination from the cytoplasmic membrane (CM) (Komeili *et al.*, 2006).

For maximum sensitivity of magnetic orientation, magnetosomes are organized within single or multiple chains, which represent one of the highest structural levels found in a prokaryotic cell. However, a string of magnetic dipoles has an immanent tendency of collapsing to lower its magnetostatic energy unless it is properly stabilized (Kirschvink, 1982; Kobayashi *et al.*, 2006). Recently, it has been found that the assembly and maintenance of magnetosome chains is governed by dedicated cellular structures. Two complementary studies investigated chain formation in the two related magnetic bacteria MSR and AMB by cryo-electron tomography (CET) (Komeili *et al.*, 2006; Scheffel *et al.*, 2006). CET has emerged as a powerful technology for bridging the gap between protein-protein interactions and cellular architecture (Lučić *et al.*, 2005; Li and Jensen, 2009; Milne and Subramaniam, 2009). In CET, cells are embedded in vitreous ice in a close-to-native state, thereby avoiding artifacts typically associated with conventional electron microscopy. CET analysis of MSR and AMB demonstrated a cytoskeletal

For Peer Review

network of filaments, 3-4 nm in diameter, which traverse the cells adjacent to the CM. Magnetosomes were closely arranged along this magnetosome-associated cytoskeleton, which has been tentatively referred to as ”magnetosome filament” (MF) (Frankel and Bazylinski, 2006). It was speculated that magnetosome filaments might be encoded by the *mamK* gene because of its sequence similarity to other cytoskeletal proteins (Grünberg *et al.*, 2004; Schüler, 2004b), which together with other genes relevant for magnetosome formation is part of the large *mamAB* operon in all analyzed MTB (Grünberg *et al.*, 2001; Jogler *et al.*, 2009a; Jogler and Schüler, 2009; Nakazawa *et al.*, 2009; Murat *et al.*, 2010). MamK proteins form a distinct and coherent branch within the large superfamily of prokaryotic actin-like proteins (Alps), which perform diverse functions in cell shape determination, establishment of polarity, cell division, chromosome segregation, and plasmid partition (Carballido-Lopez, 2006; Derman *et al.*, 2009).

Because of the difficulties with genetic manipulation of MTB, a *mamK* deletion mutant has so far been available only in AMB (Komeili *et al.*, 2006). AMBΔ*mamK* cells had lost their coherent chain-like structure. Instead, groups of few (two to three) neighboring magnetosomes were separated by large gaps and appeared dispersed throughout the cell (Komeili *et al.*, 2006). Cytoskeletal magnetosome filaments could no longer be identified in tomograms of mutant cells, indicating that MamK in fact might be the structural element of the magnetosome-associated cytoskeleton. Similar to MreB and other Alps, MamK fusions to GFP displayed a filament-like organization *in vivo* and appeared as spiral or straight lines in cells of AMB (Dye *et al.*, 2005; Pradel *et al.*, 2006). MamK-GFP of AMB expressed in *E. coli* formed straight filaments, which were structurally and functionally distinct from the known MreB and ParM filaments

For Peer Review

(Carballido-Lopez and Errington, 2003; Pradel *et al.*, 2006). Recombinant MamK of *M. magnetotacticum* MS-1 (in the following referred as MS) *in vitro* polymerized into long straight filamentous bundles in the presence of a non-hydrolyzable ATP analogue (Taoka *et al.*, 2007). In the related magnetic bacterium MSR MamK was shown to interact with the acidic repetitive MamJ protein, which was demonstrated to be another key player of magnetosome chain assembly (Scheffel *et al.*, 2006; Scheffel and Schüler, 2007). A deletion mutant of *mamJ* did no longer produce straight magnetosome chains, but magnetite crystals were found arranged in compact clusters (Scheffel *et al.*, 2006; Scheffel and Schüler, 2007), whereas empty vesicles and immature crystals are scattered throughout the cytoplasm and detached from the magnetosome filaments, which were still present within MSR∆*mamJ* cells.

One obvious model that was suggested from these data is that MamJ connects magnetosomes to the cytoskeletal MF formed by MamK, which mechanically stabilizes the magnetosome chain and prevents it from collapsing (Komeili, 2006; Komeili, 2007; Scheffel and Schüler, 2007). According to this model, loss of either MamK or MamJ should result in an essentially identical phenotype, which is the abolishment of chain formation and agglomeration of magnetosome particles. However, the reported phenotypes of the MamJ deletion in MSR (agglomerated magnetosomes) and the MamK deletion in AMB (dispersed magnetosomes) were strikingly distinct. This raised the question, whether the MamJ and MamK proteins perform different or additional functions in different species of MTB, and whether the observed phenotypic differences are due to species-specific modes of chain formation caused by different genetic control in the two strains used in the two studies (Jogler and Schüler, 2007; Komeili, 2007). In a very recent study, a second actin-like protein was discovered in the genome of AMB that

For Peer Review

shares 54.4% identity with MamK and is encoded within a genomic islet outside the MAI (Rioux *et al.*, 2010). Like MamK, this MamK-like protein was also demonstrated to form filaments both *in vivo* and *in vitro*, and it was speculated that the presence of this second *mamK*-like gene might account for the variable phenotype of the Δ*mamK* mutant in AMB (Rioux *et al.*, 2010).

To reconcile these conflicting observations and to further clarify the role of MamK, we characterized in detail a *mamK* deletion mutant of MSR by TEM and CET. We show that in contrast to AMB, MamK of MSR is not required for chain formation. However, the absence of magnetosome filaments results in a pleiotropic phenotype displaying shorter and fragmented chains that are displaced from their usual midcell localization. In addition, mutants are also impaired in magnetite formation. Our results suggest that MamK has a role in magnetosome chain positioning and MM vesicle formation, and loss of MamK may have distinct effects in different bacteria depending on the genetic context.

For Peer Review

## Results

### Characterization of an unmarked, in-frame Δ*mamK* mutant of *M. gryphiswaldense*

We generated an unmarked, in-frame *mamK* deletion mutant of *M. gryphiswaldense* (MSR), in the following referred to as MSRΔ*mamK*. Under standard conditions (microaerobic, 30 °C) cells of MSRΔ*mamK* strain exhibited morphology (Fig. 1), as well as growth and motility apparently identical to the wildtype (WT). Whereas single crossover insertants of pEK32 were deficient in magnetite crystal formation, MSRΔ*mamK* cells formed magnetosomes and aligned to magnetic fields. However, magnetic orientation of mutant cultures was markedly weaker than the WT as indicated by lower $C_{mag}$ values (1.08 vs. 1.44 in the WT). Measurement of ~ 590 magnetosomes from ~ 30 cells revealed that the magnetite crystals were unaffected in shape and size, and the mean crystal diameter of 34 nm was essentially identical to that of the WT (33 nm). However, on average MSRΔ*mamK* cells contained substantially fewer magnetosomes (19.7 crystals) per cell than WT cells (35.3 crystals) (Fig. 1D*iv*) grown under identical conditions, which was also consistent with a reduced iron accumulation of mutant cells (30.4 µg/mg vs. 51.7 µg/mg dry weight in the WT, Fig. 1D*v*).

Chain formation was assessed by TEM with respect to the average number of chains per cells, the average length (i. e. the number of particles), and the average distance between neighboring particles. A chain was defined empirically by a minimum number of 10 magnetosomes that showed a linear alignment, and which were interspaced by not more than ~ 50 nm from each other. Within this distance magnetic crystals are known to interact magnetically, whereas single particles spaced by about >200 nm are magnetically uncoupled and behave as independent magnetic dipoles (Simpson, 2008; Li *et al.*, 2009). Around 70% of WT magnetosome chains had between 19 and 44

For Peer Review

147 particles, were 0.6 to 2.5 µm in length, tightly spaced (10.9 nm interparticle distance,
148 50.2 nm center-to-center distance), with smaller, apparently growing, and more widely
149 spaced magnetite particles at the ends. In 92% of the cells straight, long, and
150 continuous chains were positioned at midcell (Fig. 1C*iii*). Ectopic (e. g. terminal) chain
151 localization or fragmented chains (6%) were found only occasionally. However, in about
152 17% of the WT cells 2-3 parallel chains were observed (Fig. 1A*i-ii*).
153 In contrast, MSRΔ*mamK* cells displayed a distinct and much more inconsistent pattern
154 of magnetosome chain configurations. A fraction of cells had lost their coherent, tightly
155 spaced chain-like structure, but instead magnetosomes were dispersed along a linear
156 axis throughout the cells and spaced by distances up to ~ 920 nm (Fig. 1B, C).
157 However, this pattern, which was somewhat reminiscent to the described phenotype of
158 Δ*mamK* in AMB (Komeili *et al.*, 2006) was found in only 18% of the cells (Fig. 1B*ii*).
159 Instead, the major fraction of cells still formed single or multiple tightly spaced chains. A
160 minor fraction (5%) of the MSRΔ*mamK* cells exhibited chains similar to those in the WT
161 (i. e., one single, tightly spaced chain with >10 magnetosome positioned at midcell; Fig.
162 1C*iii*). In the majority of cells, however, chains were aberrant with respect to their
163 number, length, and position. For example, the occurrence of fragmented chains with
164 multiple (up to 4) subchains was increased (average 1.38 chains per MSRΔ*mamK* cell)
165 compared to the WT (1.19 per cell). Individual fragmented chains on average were
166 significantly shorter (14.2 particles in MSRΔ*mamK* vs. 26.1 in the WT), and 29% of the
167 cells had chains with fewer than 10 particles, compared to only 2% in the WT. Notably,
168 parallel chains that were frequently present in WT cells, were never observed in
169 MSRΔ*mamK* cells. The position of magnetosome chains within cells was estimated by
170 dividing the cells into three equal sectors to distinguish between midcell and terminal

For Peer Review

localization. A midcell localization of the chain was observed in only 43% of MSRΔ*mamK* cells (WT: 92%), whereas in the majority of mutant cells the chains were located closely to the cell poles (Fig. 1C*i-ii*).

We and others had observed previously that purified magnetosome particles from WT cells tend to form chains *in vitro* as long as the particles are enveloped by an intact magnetosome membrane (MM) (Grünberg *et al.*, 2004; Kobayashi *et al.*, 2006; Scheffel *et al.*, 2006; Taoka *et al.*, 2007; Li *et al.*, 2009). To test whether the loss of MamK, which is associated with the MM of MSR (Fig. S1), had an effect on the integrity of the MM, and consequently, on chain formation *in vitro*, magnetosome particles purified from mutant and WT cells were investigated by TEM. Isolated mutant and WT magnetite crystals were surrounded by a MM-like organic layer of identical thickness (8-12 nm) and appearance as reported previously (Gorby *et al.*, 1988; Schüler, 2004a; Taoka *et al.*, 2006) with junctions that interconnected the individual particles (Fig. S2). Similar like WT magnetosomes, isolated mutant magnetosomes had a tendency to form chains as observed before (Grünberg *et al.*, 2004) (Fig. S2*iii-iv*).

**Complementation analysis: MamK$_{MSR}$ and MamK$_{AMB}$ are functionally equivalent**

Immunodetection revealed that MamM and MamB, whose genes are located 338 and 7192 bp downstream of *mamK* within the *mamAB* operon, respectively, were expressed at WT levels in the mutant strains (data not shown), indicating that *mamK* deletion had no polar effects. To further preclude second-site mutations, we analyzed cells transcomplemented with a functional *mamK* gene. Cloning and expression of the 1044 bp *mamK*$_{MSR}$ gene under control of the native P$_{mamAB}$ promoter (Lang *et al.*, 2009) in pEK36 resulted in MamK expression comparable to WT levels (data not shown) upon

For Peer Review

transfer into MSRΔ*mamK*. In addition, also magnetite formation, iron accumulation and chain formation were restored, albeit to a lower extent than in the WT (Fig. 1D*iv-v*, 4*iv*). To answer the question whether observed differences in WT and Δ*mamK* phenotypes between AMB and MSR might be due to sequence divergence of MamK orthologs, we also tested transcomplementation by $mamK_{AMB}$, and in addition by $mamK_{MS}$ (*M. magnetotacticum* MS-1). Plasmids pEK37and pEK35 carrying $mamK_{AMB}$ and $mamK_{MS}$, respectively, were conjugated into MSRΔ*mamK*. Magnetosome numbers, iron accumulation, $C_{mag}$ and chain formation were restored by MSRΔ*mamK*+pEK35 (data not shown) and MSRΔ*mamK*+pEK37 (Fig. 1D*iii-v*) at comparable levels, indicating that $mamK_{MS}$ and $mamK_{AMB}$ are functionally equivalent to $mamK_{MSR}$ and can substitute its function in MSRΔ*mamK* cells. We also investigated the effect of MamK overexpression by cloning of $mamK_{MSR}$ on pEK33 under control of the strong MSR promotor p*mamDC* (Lang *et al.*, 2009). Transmission electron micrographs revealed long, straight WT-like magnetosome chains in MSR cells expressing *mamK* from pEK33, and filaments of similar abundance, length, and thickness were visible within 3D maps. Likewise, cells displayed similar magnetosome numbers (Fig. 1D*i-v*) and magnetic orientation (WT $C_{mag}$=1.47, WT + pEK33 $C_{mag}$=1.50), indicating that moderate overexpression of *mamK* has only minor effects on magnetosome chain formation (Fig. S3).

**Intracellular localization of MamK**

Plasmids harboring various MamK-EGFP fusions were expressed in WT and several mutant backgrounds. Functionality of fusions was verified by partial restoration of WT-like phenotype upon expression of pAS_K, pAS_K1, pAS_K2 and pEK42 in MSRΔ*mamK*. Fluorescence microscopy revealed distinct localization patterns from

For Peer Review

linear to helical filaments in all tested MamK-EGFP fusions. However, the respective patterns were dependent on the length of the linker between EGFP and MamK: Expression of pAS_K1 harboring a C-terminal MamK-GSI-EGFP (Fig. 2*i*-*ii*) fusion, and pAS_K2 harboring an N-terminal EGFP-SAI-MamK fusion (data not shown) resulted in a linear fluorescence signal of about half the cell length that was restricted to midcell in *E. coli* and MSR, similar as observed in other studies (Pradel *et al.*, 2006). In contrast, WT+pAS_K harboring a N-terminal EGFP-LCLQGE-MamK displayed a linear-to-helical fluorescence pattern spanning from pole to pole throughout the entire cell, and occasionally forming loops (Fig. 2*iii*). A similar pattern was also observed if pAS_K and pEK42 were expressed in MSRΔ*mamK*, the non-magnetic mutant strain MSR-1B lacking most magnetosome genes by deletion (Schübbe *et al.*, 2003; Ullrich *et al.*, 2005), and *E. coli* (Fig. 2*iv*-v*iii*). Previous experiments indicated that MamK interacts with the acidic MamJ protein (Scheffel *et al.*, 2006; Scheffel and Schüler, 2007), but the filamentous localization of MamK was independent from MamJ (as demonstrated by expression in Δ*mamJ* strain) and other magnetosome genes (as demonstrated by expression in MSR-1B) (Scheffel *et al.*, 2006). Therefore, we asked whether localization of MamJ was on the other hand dependent on the presence of MamK. Expression of pAS_J harboring a MamJ-EGFP fusion in MSRΔ*mamK* abolished its filamentous localization, but instead resulted in a punctual, cytoplasmic fluorescence signal, similar as the localization of MamJ-EGFP previously detected in MSR-1B (Scheffel *et al.*, 2006)(Fig. 2*ix*-*x*). This indicates that proper MamJ localization requires the presence of MamK. Since the linear to helical localization of EGFP-MamK (pAS_K, pEK42) was also observed in *E. coli* and *M. gryphiswaldense* MSR-1B backgrounds (Fig. 2*vii*-*viii*), this demonstrates that the filamentous localization is an intrinsic property of EGFP-

For Peer Review

MamK$_{MSR}$, which does not require the presence of other magnetosome proteins. Expression of pAS_K in AMB resulted in the same filamentous signal pattern, however, spiral localization was absent (Fig. 2*xi*).

Spontaneous formations of spheroplasts ("coccoid bodies") can be regularly observed in aging cells of *M. gryphiswaldense* and other magnetospirilla (Balkwill *et al.*, 1980; Schüler and Köhler, 1992). Interestingly, in such spheroplast cells EGFP-MamK (pAS_K) did no longer localize within linear filaments, but instead yielded a ring-like fluorescence signal closely beneath the cell periphery, which is consistent with the peripheral ring-like, bent appearance of the magnetosome chains in such a cell as shown by fluorescence microscopy and TEM (Fig. 2*xii*-*xiii*).

**Cryo-electron tomography (CET)**

Previous CET analyses of magnetosome chain topology in AMB and MSR were limited to only single or a few cells (Komeili *et al.*, 2006; Scheffel *et al.*, 2006). Therefore, we analyzed chain assembly and magnetosome filaments in greater detail in a larger number of WT and MSRΔ*mamK* cells of MSR. Filaments accompanying the magnetosome chains were identified in 16 of 28 of all analyzed tomographic volumes from WT cells (Fig. 3*ii*-*viii*), and 2 of 10 analyzed MSRΔ*mamK* cells complemented with pEK42 (*mamK*$_{MSR}$, Fig. 4*iv*) and pEK34 (*mamK*$_{AMB}$). Since tomograms at the recorded magnification are limited in the field of view, they represent only a fraction of the whole cell. Moreover, some information is not accessible due to the limited tilt range and the resulting missing wedge. Therefore it is possible that filaments in the other WT and transcomplemented cells escaped detection if localized perpendicular to the tilt-axis. Individual filaments, which were 3 - 6 nm in diameter and 0.5 - 1 µm in length,

For Peer Review

occasionally formed bundles of 2 - 4 filaments that were ~ 20 nm in diameter and approximately 1 µm long (Movie S1). However, since filaments were not always within the same z-plane, their total dimensions can only be roughly estimated. Detected filaments were localized within the cytoplasm in close proximity to MM vesicles. Although the magnetosome chains were predominantly found at midcell, empty vesicles and filaments were also present in 100 – 300 nm vicinity to the inner membrane of the cell pole. However, we were unable to detect direct connections or discern distinct structures where filaments insert into the polar membrane. This was partially due to the presence of complex ordered structures resembling arrays of chemoreceptors (Briegel *et al.*, 2009), which were located closely beneath the polar membrane (Fig. 3*vii*-*viii*). Analysis of different CET datasets determined an array length of ~ 28 nm and a lattice distance of ~ 11 nm (Fig. 3*viii*, insets). Notably, in some cells filaments seemed to be connected laterally to the CM.

A couple of WT and transcomplemented cells were tomographed in state of early (Fig. 3*iv*-*v*), and late division (Fig. 4*iv*). According to those tomograms, the MF traverse the entire cell before septum formation, which remarkably might occur asymmetrically from only one side (Fig. 4*iv*). During later division the magnetosome chain, and likely also the magnetosome filament may be split into two parts (Fig. 3*iv*-*v*, 4*iv*). However, due to the potential risk of technical artifacts these observations require future verification. Interestingly, two distinct filaments were detected in fig. 4*iv* within this cell. This was not observed in the analyzed WT cells and might be the result of *mamK* expression from pEK42.

As in conventional micrographs, tomograms of WT cells frequently showed two parallel chains of particles that were aligned opposite to each other along the filaments (Fig. 1A*i*,

For Peer Review

3*i*-*v*). In contrast, we failed to detect parallel chains in any of the 15 analyzed MSRΔ*mamK* tomograms, which always contained only one linear string of crystals per analyzed section.

Sometimes filaments with association to the CM were detected, where magnetosomes were absent or sparse (Fig. 3*iii*). Whereas the number of magnetite crystals was significantly lower in MSRΔ*mamK*, the proportion of empty vs. filled vesicles per tomographed area was not increased. Even though the absolute enumeration of vesicles per cell is not possible due the limited analyzed area and technical limitations (e.g. limited tilt range, missing wedge), the total number of MM vesicles (empty or filled) per viewed section was also decreased in the mutant. If all tomograms of central sections at identical magnification were taken into account under the assumption that they may represent comparable, randomly chosen areas at midcell from the WT (15 cells) and MSRΔ*mamK* (8 cells) cells, the average number of all vesicles were 21.6 (WT) vs. 14.8 in the mutant, respectively, implying that the formation of MM vesicles is affected in the mutant.

MM vesicles were predominantly found in close contact with the CM. In several cells, empty MM vesicles were detected that were invaginating from the CM, apparently with the MM forming a continuum with the CM (Fig. 3*iv*, inset). The size of empty or partially filled vesicles varied between 13.4 and 33.5 nm. However, vesicle dimensions were not strictly correlated with the presence or absence of growing immature crystallites, as larger vesicles (18 - 33.5 nm) devoid of crystals as well as smaller vesicles harboring small crystallites were apparent in the analyzed tomograms.

**Effect of MSRΔ*mamK* on dynamic assembly of magnetosome chains**

For Peer Review

Deletion of *mamK* did not result in agglomeration of magnetosomes, but mutant cells still maintained a chain-like configuration. We therefore reasoned that instead merely providing a backbone or scaffold that mechanically stabilizes the magnetosome chain, the primary function of MamK might be rather in the control of the dynamic positioning and concatenating the individual particles during chain assembly and cell division as speculated before (Frankel and Bazylinski, 2006; Pradel *et al.*, 2006). For clarification, we undertook a growth experiment in which magnetite synthesis was induced in growing MSRΔ*mamK* and WT cells by the addition of iron to previously non-magnetic, iron-starved cells. As shown in Fig. 5, both WT and MSRΔ*mamK* cells started to form magnetite after addition of 50µM Fe(III)-citrate, and small (10 – 20 nm) crystallites could be first detected after 30 min. As in previous induction experiments (Scheffel *et al.*, 2006; Faivre *et al.*, 2007), initiation of magnetosome formation took place usually at few locations close to the cell periphery and scattered throughout the cell in WT and MSRΔ*mamK.* During the first 80 min magnetite biomineralization proceeded at similar rates in both strains. After about 100 min, magnetite formation of the mutant then lagged behind the WT, resulting in a lower magnetic orientation for the MSRΔ*mamK* over the remaining 200 min (Fig. 5). After 90 min irregular chains of magnetosomes became apparent at different loci in both mutant and WT cells. However, while WT cells formed the typical linear, and sometimes parallel chain fragments already located at midcell, chains in induced MSRΔ*mamK* mutant cells were displaced, short and more distorted than in those WT cells. After 120 and 300 minutes, further development of WT chains resulted in gradual extension and midcell localization, whereas in MSRΔ*mamK* cells fragmented, displaced chains were formed.

For Peer Review

## Discussion

Previous studies had suggested that the actin-like protein MamK is required for magnetosome chain assembly of AMB by aligning these organelles within the cell (Komeili *et al.*, 2006; Pradel *et al.*, 2006). However, the phenotype of a Δ*mamK* mutant of MSR generated in this study argues against an essential role in chain formation in this organism, since in spite of the absence of filamentous structures mutant cells are still able to form linear and coherent chains, albeit with reduced lengths and ectopic positions. For the assembly of an functional magnetosome chain, individual magnetite crystals have to be (i) aligned along a common linear axis, (ii) concatenated (i. e. by bringing newly synthesized particles to the nascent, tightly spaced magnetosome chain), and finally, (iii) chains have to positioned properly at their usual midcell localization. Instead merely providing a backbone or scaffold that mechanically stabilizes magnetosome chain, our data support speculations that MamK might be involved in sorting, concatenating and intracellular positioning of the magnetosome chain (Pradel *et al.*, 2006; Jogler and Schüler, 2009). On the other hand, the fact that a small percentage of Δ*mamK* cells still form long chains does not necessarily indicate that MamK has no scaffolding role at all, but just could mean that it cannot be the only factor promoting chains.

Our induction experiments show that MSRΔ*mamK* cells are also still able to assemble short, but coherent chains from dispersed magnetosome particles if challenged with the *de novo* synthesis of magnetite particles in non-magnetic, iron-starved cells undergoing cell division. This raises the question of how these chains are maintained in MSRΔ*mamK* mutants against their immanent tendency to agglomerate. Several mechanisms for chain formation have been suggested. In AMB chain initiation starts

For Peer Review

with the simultaneous formation of multiple, adjacent magnetosomes (Komeili *et al.*, 2004; Li *et al.*, 2009). In marked difference, magnetite biomineralization in MSR is initiated at multiple sites dispersed over the entire cell (Scheffel *et al.*, 2006) before eventually becoming concatenated into the mature coherent chains located at midcell, which suggests a control over dynamic localization and intracellular positioning of magnetosomes in this organism. When magnetic crystals continue to grow, increasing magnetostatic interactions between adjacent particles force them into close contact, which is then further stabilized by interactions through MM constituents. In the absence of the "bead-on-a-string" like alignment along the MamK filaments, connections between the invaginating MM vesicles and the CM may be sufficient to maintain the linear arrangement of subchains in MSRΔ*mamK*. In addition to the cytoskeletal magnetosome filament, an elusive sheath-like structure has been postulated that may hold magnetosome chains together and in place within the cell (Kobayashi *et al.*, 2006; Taoka *et al.*, 2006). However, in our extensive CET studies we failed to detect any indications for the existence of such an intracellular structure.

Like in AMB, deletion of the *mamK* gene resulted in the complete absence of magnetosome filaments. In addition, we were unable to detect any other filament-like structures in MSRΔ*mamK* cells. This is interesting, as MSRΔ*mamK* cells are likely to contain further cytoskeletal structures formed by other filamentous proteins, such as MreB and FtsZ, which are encoded in the genome of MSR. In a study on *C. crescentus*, in which the formation of MreB filaments was inhibited by A22 treatment, similar filaments, which were speculated to be FtsZ, were still detectable by CET (Li *et al.*, 2007). Our failure to detect them thus might indicate that other cytoskeletal structures are way less abundant than MamK filaments within the cell.

For Peer Review

Complementation of the MSRΔ*mamK* mutant not only with $mamK_{MSR}$, but also with $mamK_{AMB}$ and $mamK_{MS}$ did restore chain formation and the presence of magnetosomal filaments, indicating that these *mamK* allels have equivalent functions and can substitute each other. However, despite the morphological and ultrastructural resemblance of the two organisms, the phenotypes of *mamK* mutants are distinct between MSR and AMB. Whereas the effect on chain assembly is less pronounced in MSRΔ*mamK* than in AMB1Δ*mamK*, in which the mutant lacked the long, highly organized chains seen in WT (Komeili *et al.*, 2006), loss of MamK in MSR has several additional, pleiotropic effects. These differences do not result from different growth conditions, as MSR grown in MSGM (i. e. the genuine AMB medium) displayed the same morphology and magnetosome organization as in FSM medium (data not shown). On the other hand, WT AMB cells grown in FSM medium under identical conditions as MSR display a distinct chain configuration that is characterized by fairly loose, widely spaced chains that may extend through the entire cell (Fig. S4), compared to the midcell localization of densely spaced MSR chains (Fig. 1A), and it has been recently argued by Rioux *et al.* that the fraction of misaligned magnetosome chains in AMB1Δ*mamK* may be well within the variability usually observed in the WT strain (Rioux *et al.*, 2010). This relatively weak phenotype and the differences between MSR and AMB might be explained by the fact that only 52% of all genes are shared between the two strains (Richter *et al.*, 2007). In fact, in the recent study by Rioux *et al.* a second mamK-like gene was discovered outside the MAI in an islet together with 6 additional magnetotaxis related genes (Rioux *et al.*, 2010). These findings support the idea that the observed differences between AMB and MSR and their *mamK* mutants are due to a different genomic context.

For Peer Review

Therefore, only a double deletion mutant of the *mamK*-like gene in addition to Δ*mamK* will reveal a more conclusive picture about MamK function in AMB.

One of the various effects of the *mamK* deletion in MSR is the formation of multiple, fragmented chains, which are strongly reminiscent to the subchains observed by Li *et al.* in experiments, in which magnetite formation was induced in aerobically grown non-magnetic cells of AMB by a shift to microaerobic incubation (Li *et al.*, 2009). Each of these subchains behaved as an ideal uniaxial single-domain particle with extremely weak magnetostatic interactions between subchains (Li *et al.*, 2009). Another distinctive feature of the MSR mutant is that the chains are displaced from their usual midcell location, which indicates that MamK is involved in positioning of magnetosomes by an as yet unknown mechanism. It has been speculated that positional information might be provided possibly by interaction with the divisome machinery that regulates proper cell division and determines septum formation (Schüler, 2008; Adams and Errington, 2009). This hypothesis has been further stimulated by the fact that a second *ftsZ*-like gene has been identified in the *mamXY* operon of MSR (Richter *et al.*, 2007). A putative chimeric protein was found within a metagenomic clone, in which a MamK-like domain is coupled to an FtsZ-like domain (Jogler *et al.*, 2009b). A recent study has shown that the second FtsZ-like protein in MSR is not involved in cell division but had rather an effect on biomineralization and, apparently, also on chain assembly (Ding *et al.*, 2009). So far, it still remains to be analyzed whether this or the genuine FtsZ has an effect in providing information about midcell position.

Previous studies of $MamK_{AMB}$ localization by Komeili *et al.* revealed that a C-terminal GFP fusion appeared in straight lines extending across most of the cell approximately along its inner curvature, consistent with the magnetosome-associated filaments in both

For Peer Review

433 localization and extent (Komeili *et al.*, 2006). CET revealed networks of long filaments
434 200 to 250 nm in length running parallel along the chain of an AMB WT cell. At any
435 position within the chain, up to seven of these filaments flanked the magnetosome with
436 no obvious spatial pattern (Komeili *et al.*, 2006). In contrast, fluorescence microscopy in
437 our study revealed a more variable localization pattern of $MamK_{MSR}$ depending on the
438 particular GFP fusion and linker length. Variable fluorescence patterns were also
439 detected for other actin-like proteins like ParM and MreB (Jones *et al.*, 2001; Møller-
440 Jensen *et al.*, 2002), as incorporation of EGFP into a polymeric structure might affect
441 MamK tertiary structure. Thus, a longer linker might provide sterical freedom required for
442 its native localization. In addition, different linkers might affect the stability of EGFP
443 fusions, and therefore, the distinct localization of the MamK fusions might also be
444 function-unrelated. Although MamK-EGFP fusions (pAS_K1/2), which show midcell
445 fluorescence, also seem to complement the deletion of *mamK*, the pole-to-pole
446 localization observed for EGFP-MamK (pAS_K, pEK42) is more consistent with the
447 polar localization of MF bundles observed by CET, and also with the observation by
448 Pradel *et al.* that one extremity of $MamK_{AMB}$ was located at the pole if expressed in *E.*
449 *coli* (Pradel *et al.*, 2006; Pradel *et al.*, 2007). It has been also suggested by these
450 authors that MamK might somehow be involved in magnetoreception, possibly by
451 interaction with other polar components (IcsA) (Pradel *et al.*, 2006). Our finding that
452 extremities of MamK in some MSR cells extend towards arrays of chemoreceptors
453 would support a possible interaction between *mamK* and these structures in signal
454 transduction.
455 It has been demonstrated previously that MamK interacts with MamJ, but MamJ is not
456 required for MamK filament formation (Scheffel *et al.*, 2006; Scheffel and Schüler, 2007).

For Peer Review

We found that on the other hand MamK is required for the filamentous localization of MamJ-EGFP (Fig. 2*ix-x*), which is abolished in the MSRΔ*mamK* mutant. Previous studies have suggested that MamJ attaches magnetosomes to filaments formed by MamK by direct interaction (Scheffel and Schüler, 2007). If this would be the only MamJ function, then loss of either MamJ or MamK would be expected to result in essentially identical phenotypes, which is the collapse of chains and agglomeration of magnetosomes. As chain configuration, however, is maintained even in the absence of MamK, but not MamJ, the mode of chain stabilization by MamJ cannot exclusively be accomplished by MamK interaction, but has to involve other, so far unknown mechanisms as well.

MSRΔ*mamK* chains are also shorter, presumably as a consequence of the decreased numbers of magnetite crystals in the mutants. At this point, the reason for this unexpected effect on magnetosome formation is not clear. It has been suggested that MamK could act through establishment of magnetosome biogenesis factors (Komeili, 2007). This might be, for example, by mediating the recruitment of other proteins required for biomineralization to the MM. A role in the recruitment and positioning of particular proteins has been demonstrated for other Alps and tubulin-like proteins, such as FtsZ, ParM and MreB, in *B. subtilis* and *E. coli* (Salje and Löwe, 2008; Adams and Errington, 2009; Gamba *et al.*, 2009; Vats *et al.*, 2009). However, a preliminary comparative analysis of the MM between the mutant and the WT revealed virtually the same band patterns in SDS-PAGE experiments (data not shown). Intriguingly, our data imply that the number of magnetosome membrane vesicles is higher (21.6) in tomograms of the WT compared to 14.8 in the mutant, and the reduced number of MM

For Peer Review

vesicles in the mutant might be the reason why less magnetosome crystals are formed in cells devoid of MamK.

Our extensive CET analysis of > 40 WT and mutant cells also revealed several previously unrecognized ultrastructural features with relevance for magnetosomal organelle formation. For example, we have shown that, like in AMB the MM in MSR invaginates from the CM and at least transiently forms a continuum between the two membranes (Komeili *et al.*, 2006), indicating that the mechanisms of intracellular differentiations are similar between these organisms. In addition, we found that in the WT formation of two parallel chains is rather common, which was never observed in MSRΔ*mamK* cells. The reason for the formation of multiple chains in the WT is not entirely clear, but it can be speculated that MamK filaments may have a strong affinity for binding MM vesicles, possibly by its interaction with MamJ and other proteins, and thus tend to gather magnetosomes within their vicinity.

In conclusion, our data argue for a function of MamK in positioning and concatenating magnetosome chains rather than merely providing a rigid scaffold for chain alignment. Our results further suggest that the role of MamK is likely to be more complex and somewhat distinct from previously reported models that were mostly inferred from the single *mamK* deletion in AMB (Komeili *et al.*, 2006; Rioux *et al.*, 2010). At this point, the precise mechanisms by which magnetosome chains are positioned by MamK remains elusive and will require further investigation of interaction with and localization of further constituents of the magnetosome assembly and vesicle formation machinery.

**Acknowledgement**

For Peer Review

We are grateful to Günter Pfeifer (MPI of Biochemistry) for help with the TEM. This work was supported by the Max Planck Society and the Deutsche Forschungsgemeinschaft (Schu1080/9-1 and 10-1).

For Peer Review

# Experimental procedures

**Bacterial strains, media and magnetosome isolation**

Strains *M. magnetotacticum* AMB-1 (AMB) and *M. gryphiswaldense* MSR-1 (MSR) were grown in modified liquid FSM medium and LIM (Low iron media, modified FSM) (Faivre *et al.*, 2007). Modified magnetic spirillum growth medium (MSGM) (Blakemore *et al.*, 1979; Komeili *et al.*, 2004)(50 µM ferric citrate instead of ferric malate) was alternatively used where indicated. Growth of *Escherichia coli* strain BW29427 (Tab. 1) was accomplished in lysogeny broth (LB) supplemented with 1 mM DL-$\alpha$,$\varepsilon$-diaminopimelic acid (Sigma-Aldrich, Switzerland). Culture conditions for *E.coli* strains were as described (Sambrook and Russel, 2001). Magnetosomes were isolated from microaerobically grown 5l cultures as described elsewhere (Grünberg *et al.*, 2004; Ohuchi and Schüler, 2009). Optical densities and $C_{mag}$ values of MSR cultures were measured turbidimetrically at 565 nm with immotile cells inactivated by the addition of formaldehyde (Fluka, Switzerland) to a final concentration of 0.1% prior to the measurement (Scheffel *et al.*, 2006).

**DNA techniques and Southern Blot**

Total DNA from all strains used in this study was isolated as described previously (Marmur, 1961; Grünberg *et al.*, 2001). Genetic constructs used to generate the MSRΔ*mamK* deletion were amplified using standard PCR procedures. The primers and plasmids used in this study are shown in Table 1. Primer sequences for amplification of DNA fragments from MSR were deduced from GenBank sequence deposition BX571797. The primer pairs used for the amplification of *mamK* from *Magnetospirillum* strains AMB and MS were deduced from sequence deposition NC_007626 and

For Peer Review

NZ_AAAP01003824.1, respectively. For sequencing, BigDye terminators v3.1 (Applied Biosystems, Darmstadt, Germany) were used. Sequence data were analyzed with Lasergene 6 (DNAstar, Inc., Madison, WI) and MacVector 7.2.3 (Oxford Molecular, Ltd., Oxford, United Kingdom) programs. Southern blots were performed by standard procedures as described previously (Ullrich *et al.*, 2005) (Fig. S5).

**Construction of an unmarked in-frame *mamK* deletion mutant**

Gene deletion was accomplished via homologous recombination of up- and downstream *mamK* flanking sequence in pEK32 with the MSR chromosome. A 2003 bp upstream and a 2009 bp downstream *mamK* flanking region were amplified with primer pairs EK2_K_u_f /EK_K_u_r and EK_K_d_f/EK2_K_d_r. The fragments were fused by cloning into the *Xba*I and *BamH*I restriction sites of pK19*mob*GII vector, resulting in pEK32. Plasmids were transferred into *M. gryphiswaldense* by biparental conjugation and screening was performed as previously described (Schultheiss *et al.*, 2004). Screening for the *gusA* marker (Katzen *et al.*, 1999) revealed 8 $Kan^R$ insertion mutants occurring with a frequency of $1.7x10^{-7}$ on X-Gluc (5-Bromo-4-Chloro-3-Indolyl-β-D-glucuronic acid, 0.5 mM) containing solid FSM plates. After 2 passages for 3 days in 300 µl liquid culture and subsequent 1 day in 10 ml (~ 5 generations), an incubation for 10 days on solid FSM at 30 °C under microoxic conditions was performed. Screening by PCR of 24 white colonies for putative double crossover resolvants revealed 8 positive candidates that were $gusA^-$ and $Kan^S$. Double crossover mutants were obtained at a final frequency of $2.6x10^{-3}$. Successful unmarked in-frame deletion of *mamK* was confirmed by PCR and Southern blotting using a 816 bp DNA probe amplifying parts of *mamJ* and *mamK* gene of MSR with primer pairs EK_K_f/ EK_probeK02_r (Fig. S5).

For Peer Review

One clone named MSRΔ*mamK* was selected for further analysis.

**Complementation experiments**

A cloned fragment comprising an open reading frame of 1083 bp that starts with a CTG codon according to the previously deposited database sequence (CAJ30118, (Ullrich *et al.*, 2005)) was not functionally expressed (data not shown). Inspection of the aligned sequences of *mamK* nucleotide sequences of *mamK* orthologs from MSR, AMB (1044 bp, 33 nt mismatches, 90.8 % aa identity) and MS (1044 bp, 34 nt mismatches, 90.6 % aa identity) revealed a conserved ATG in all three orthologs 39 bp downstream of the predicted CTG start codon in the older database version of $mamK_{MSR}$, which hereafter was considered as the correct start codon, resulting in an open reading frame of 1044 bp as in the other strains.

The *mamK* gene was either amplified with primer pair EKmamK_F_kurz/EKmamK_R02 and the 1056 bp fragment subsequently cloned into *Nde*I and *BamH*I restriction sites of $pBBR_{PmamDC}$ generating pEK36, or with primer pair EKmamK_F02/EKmamK_R02 resulting in a 1083 bp fragment in which the start codon CTG was changed into an ATG. Likewise, the ATG defines the recognition site of 5' *Nde*I restriction enzyme. Together with the 3' *BamH*I recognition site the fragment was cloned into pBBR1p*mamAB* (Lang *et al.*, 2009) yielding pEK36 and subsequently transformed into MSRΔ*mamK* via biparental mating as described (Schultheiss and Schüler, 2003; Schultheiss *et al.*, 2004). The *mamK* of AMB was PCR amplified with primer pairs EK_mamK_AMB1_F/EK_mamK_AMB1_R2 yielding a 1056 bp fragment which was cloned into *Nde*I/ *BamH*I restriction site of pBBR1p*mamAB* or pBBRp*mamDC,* resulting

For Peer Review

in pEK37 and pEK34, respectively. Amplification and subsequent cloning of MS *mamK* into pBBR1p*mamDC* resulted in pEK35.

**Construction of Mam-EGFP fusions**

Several different *mamK-egfp* (enhanced GFP) expression fusions were constructed via fusion PCR (Ho *et al.*, 1989). The *mamK* gene of MSR (accession number CAJ30118) and *egfp* (pEGFP-N2, Clontech) were amplified using primers as described, resulting in the C-terminal MamK fusion pAS_K1 (Scheffel, 2007). For construction of the N-terminal fusion with a 6 amino acid linker sequence, primer pairs for *egfp*-gene ASEGFP_f10/ ASEGFP_r11, and for *mamK* ASmamKs_f3/ ASmamKe_r2, were used and resulted in pAS_K vector (Scheffel, 2007).

**Gel electrophoresis and Western Blot experiments**

Protein concentrations were determined with a BCA-Protein Micro assay kit (Pierce) according to the manufacturer's instructions. For one-dimensional SDS-PAGE of magnetosome-associated proteins we used the procedure of Laemmli (Laemmli, 1970). An amount of magnetosome particles or solubilisate equivalent to 6.5 µg of protein was mixed with electrophoresis sample buffer containing 2% (wt/wt) SDS and 5% (wt/vol) 2-mercaptoethanol. After boiling for 5 min, samples were centrifuged for 3 min. The supernatants were loaded onto polyacrylamide gels containing various concentrations of polyacrylamide (8 to 16%). The non-magnetic fraction of whole cells was further processed as described elsewhere (Grünberg *et al.*, 2001), and 6.5 µg protein were used for analysis on SDS gels. Western Blot experiments were performed as explained in previous work (Schübbe *et al.*, 2006). The anti-MamK primary antibody was raised by

For Peer Review

S. Schübbe as described (Schübbe, 2005).

**Fluorescence microscopy**

MSR WT and MSRΔ*mamK* bearing the plasmids pAS_J, pAS_K(1,2), were grown in 15 ml polypropylene tubes with sealed screw caps and a culture volume of 10 ml to stationary phase. The cell membranes were stained with the membrane stain FM4-64 (Invitrogen, Karlsruhe, Germany) at a final concentration of 16.4 µM, immobilized on agarose pads (FSM salts in $H_2O$, supplemented with 1% agarose), and imaged with an Olympus BX81 microscope equipped with a 100 UPLSAPO100XO objective (numerical aperture of 1.40) and a Hamamatsu Orca AG camera. Images were captured and analyzed using Olympus cell™ software.

**Transmission electron microscopy and Cryo-electron tomography**

For transmission electron microscopy (TEM) analysis, unstained cells were adsorbed on carbon coated copper grids and air-dried (Plano, Wetzlar). Bright field TEM was performed on a FEI Tecnai F20 transmission electron microscope (FEI; Eindhoven, The Netherlands) at an accelerating voltage of 200 kV. Images were captured with a FEI Eagle 4096 x 4096 pixel CCD camera using EMMenue 4.0 and FEI's Explore 3D.

For cryo-electron tomography, a FEI Tecnai F30 Polara transmission electron microscope (FEI; Eindhoven, The Netherlands), equipped with 300 kV field emission gun, a Gatan GIF 2002 Post-Column Energy Filter, and a 2048 x 2048 pixel Gatan CCD Camera (Gatan; Pleasanton, CA) was used. All data collection was performed at 300 kV, with the energy filter operated in the zero-loss mode (slit width of 20 eV). Tilt series were acquired using Serial EM (Mastronarde, 2005) and FEI's Explore 3D software.

For Peer Review

Quantifoil copper grids (Quantifoil Micro Tools GmbH, Jena) were prepared by placing a 5 µl droplet of 10 – 15 nm colloidal gold clusters (Sigma) on each grid for subsequent alignment purposes. A 5 µl droplet of a fresh MSR culture was added onto the prepared grid, and after blotting was embedded in vitreous ice by plunge freezing into liquid ethane (temperature ca. -170 °C). Single-axis tilt series for tomography were typically recorded with 2° increments over an angular range of +/- 65°. To minimize the electron dose applied to the ice-embedded specimen, data were recorded at low-dose conditions by using automated data acquisition software. The total dose accumulated during the tilt series was kept below 100 e/Å$^2$. To account for the increased specimen thickness at high tilt angles, the exposure time was multiplied by a factor of 1/cos $\alpha$. The object pixel size in unbinned images was 0.661 at a magnification of 34000 x, 0.805 at 27500 x and 0.979 at 22500 x. Images were recorded at nominal defocus values of -8 µm or -4 µm.

**Data analysis**

Three-dimensional reconstructions from tilt series were performed with the weighted back-projection method and further analysis of the tomograms was done using the TOM toolbox (Nickell *et al.*, 2005). Visualizations of the tomograms were done with Amira (http://www.amiravis.com) on 2 times binned volumes.

**Determination of iron content by atomic absorption spectroscopy (AAS)**

Cells were grown to an optical density of 0.2 and aliquots of 1 ml were taken and pelleted. After a subsequent pellet washing step in 0.5 ml 20 mM HEPES + 5mM EDTA both the supernatant (900 µl) and the pellet were supplemented with 10 µl and 100 µl 65 % nitric acid, respectively. Incubation at 98 °C for 2 h dissolved all organic material and

For Peer Review

magnetosomes, and dilutions of 1:100 and 1:1000 in $H_2O$ were analyzed by AAS (Varian AA240) using SpectrAA 240FS software version 5.01 (Varian, Australia) with the following parameters set: wavelength 248.3 nm, slit width 0.2 nm, cathode lamp current 10.0 mA.

**Table 1: Plasmids, primers and strains used in this work**

| Vector | Details | Reference | Index |
|---|---|---|---|
| pEK32 | 4kb flanking sequences of *mamK* [13] | this work | [1] |
| pEK33 | *mamK*$_{MSR-1}$ [15] | this work | [2] |
| pEK34 | *mamK*$_{AMB-1}$ [15] | this work | [3] |
| pEK35 | *mamK*$_{MS-1}$ [15] | this work | [4] |
| pEK36 | *mamK*short$_{MSR-1}$ [16] | this work | [5] |
| pEK37 | *mamK*$_{AMB-1}$ [16] | this work | [6] |
| pEK40 | *mamK*$_{MSR-1}$[16] | this work | [7] |
| pEK42 | *egfp*_LCLQGE_*mamK*short$_{MSR-1}$ [14] | this work | [8] |
| pAS_K | *egfp*_LCLQGE_*mamK*$_{MSR-1}$ [14] | (Scheffel, 2007) | [9] |
| pAS_K1 | *mamK*_GSI_*egfp* [14] | this work | [10] |
| pAS_K2 | *egfp*_SAI_*mamK* [14] | this work | [11] |
| pAS_J | *mamJ*_*egfp* [14] | (Scheffel *et al.*, 2006) | [12] |
| pK19*mob*GII | - | (Katzen *et al.*, 1999) | [13] |
| pBBR1MCS-2 | - | (Kovach *et al.*, 1994) | [14] |
| pBBRP*mamDC* | - | (Lang *et al.*, 2009) | [15] |
| pBBRP*mamAB* | - | (Lang *et al.*, 2009) | [16] |
| Primer | Sequence (5' - 3') | Restriction site | |

For Peer Review

| | | | |
|---|---|---|---|
| EKmamK_F02 | | CATATGTGGATTGATCTGTTAGC | *Nde*I |
| EKmamK_R02 | | GGATCCTCACTGACCGGAAAC | *BamH* |
| EKmamK_F_kurz | | CATATGAGTGAAGGTGAAGG | *Nde*I |
| EKmamK_R02 | | GGATCCTCACTGACCGGAAAC | *BamH* |
| EK_mamK_AMB1_F | | CATATGAGTGAAGGTGAAGGCC | *Nde*I |
| EK_mamK_AMB1_R2 | | GGATCCTCACGAGCCGGA | *BamH*I |
| EK_mamK_MS1_F | | CATATGAGTGAAGGTGAAGGC | *Nde*I |
| EK_mamK_MS1_R2 | | GGATCCTCACGAGCCGGAG | *BamH*I |
| EK2_K_u_f | TCTAGAGTAGCCGGGCCTCGCTCCTGGG | | *Xba*I |
| EK_K u_r | CCCGGGGATTGCTAACTAGTCAGGT | | *Sma*I/ |
| | | CTCTATTTATTCTTATCTTC | *Spe*I |
| EK_K d_f | ACTAGTCACGTCAAGGACCCGACTTTTG | | *Spe*I |
| EK2_K d_r | CCCGGG GGATCCATTTCCGCCTTCTTCCAGTC | | *BamH*I |
| ASEGFP_f10 | GAATTCATGGTGAGCAAGGGCGAG | | *BamH*I |
| ASEGFP_r11 | CTCGCCCTGCAGGCACAGCTTGTACAGCTCGTCCAT | | - |
| ASmamKs_f3 | | TGCCTGCAGGGCGAGCTGTGGATTGATCTGTTA | - |
| ASmamKe_r2 | | TCTAGACTACTGACCGGAAACGTCACC | *Xba*I |
| EK_K_f | | TTGCTGCTCCCGCCGTTG | |
| EK_probeK02_r | | TTGTCCAAGCCATAGCCG | |

| Name | Relevant genotype or phenotype | Construction |
|---|---|---|
| *Magnetospirillum gryphiswaldense,* Δ*mamK* | MSR-1 E10, Δ*mamK,* Rif$^r$, Strep$^r$, | this work |
| *Magnetospirillum* | Rif$^r$, Strep$^r$ derivative of | (Schultheiss *et al.*, 2004) |

For Peer Review

| | | |
|---|---|---|
| *gryphiswaldense* MSR-1 | DSM6361 (WT) | |
| *Magnetospirillum* | Rif$^r$, Strep$^r$, Δ*mamJ* | (Scheffel *et al.*, 2006) |
| *gryphiswaldense* MSR-1, | | |
| Δ*mamJ* | | |
| *Magnetospirillum* | | |
| *gryphiswaldense* MSR-1B | Rif$^r$, Strep$^r$, spontaneous | |
| | deletion mutant, | |
| | lacking 40.4 kb within MAI, | |
| | mag$^-$ | |
| | | |
| | | (Schübbe *et al.*, 2003; |
| | | Ullrich *et al.*, 2005) |
| | | |
| *Magnetospirillum* | WT | (Kawaguchi *et al.*, 1992) |
| *magneticum* AMB-1 | ATCC700264 | |
| | | |
| | | |
| *E. coli* DH5α | F$^-$ *sup*E44 DacU169 | |
| | (80*lac*ZDλacU169(Φ 80*lac*ZDM15) | |
| | *hsd*R17*rec*A1*end*A1*gyr*A96*thi*-1*rel*A1 | (Bethesda |
| | Research Laboratories, 1986) | |
| *E. coli* BW29427 | *thrB*1004 *pro thi rpsL hsdS lacZ*ΔM15 | |
| | RP4-1360Δ(*araBAD*)567Δ*dapA* | |

For Peer Review

| | |
|---|---|
| 1341::[*erm pir*(Wildtyp)]*tra* | K.A. Datsenko and B.L. Wanner (Purdue University, IN, USA) |

For Peer Review

Adams, D. W. and Errington, J. (2009) Bacterial cell division: assembly, maintenance and disassembly of the Z ring. *Nat Rev Microbiol* **7**: 642-653.

Balkwill, D., Maratea, D. and Blakemore, R. P. (1980) Ultrastructure of a magnetotactic spirillum. *J Bacteriol* **141**: 1399-1408.

Bethesda Research Laboratories (1986) BRL pUC host: *E. coli* DH5 alpha competent cells. *Focus* **8**: 1-19.

Blakemore, R., Maratea, D. and Wolfe, R. (1979) Isolation and pure culture of freshwater magnetic spirillum in chemically defined medium. *J Bacteriol* **140**: 720-729.

Briegel, A., Ortega, D. R., Tocheva, E. I., Wuichet, K., Li, Z., Chen, S., et al. (2009) Universal architecture of bacterial chemoreceptor arrays. *Proc Natl Acad Sci USA* **106**: 17181-17186.

Carballido-Lopez, R. (2006) The bacterial actin-like cytoskeleton. *Microbiol Mol Biol Rev* **70**: 888-909.

Carballido-Lopez, R. and Errington, J. (2003) A dynamic bacterial cytoskeleton. *Trends Cell Biol* **13**: 577-583.

Derman, A. I., Becker, E. C., Truong, B. D., Fujioka, A., Tucey, T. M., Erb, M. L., et al. (2009) Phylogenetic analysis identifies many uncharacterized actin-like proteins (Alps) in bacteria: regulated polymerization, dynamic instability and treadmilling in Alp7A. *Mol Microbiol* **73**: 534-552.

Ding, Y., Li, J., Liu, J., Yang, J., Jiang, W., Tian, J., et al. (2009) Deletion of the *ftsZ*-like gene results in the production of superparamagnetic magnetite magnetosomes in *Magnetospirillum gryphiswaldense*. *J Bacteriol* **192**: 1097-1105.

For Peer Review

Dye, N. A., Pincus, Z., Theriot, J. A., Shapiro, L. and Gitai, Z. (2005) Two independent spiral structures control cell shape in *Caulobacter*. *Proc Natl Acad Sci USA* **102**: 18608-18613.

Faivre, D., Böttger, L. H., Matzanke, B. F. and Schüler, D. (2007) Intracellular magnetite biomineralization in bacteria proceeds by a distinct pathway involving membrane-bound ferritin and an iron(II) species. *Angew Chem Int Ed Engl* **46**: 8495-8499.

Frankel, R. and Bazylinski, D. (2006) How magnetotactic bacteria make magnetosomes queue up. *Trends Microbiol* **14**: 329-331.

Gamba, P., Veening, J.-W., Saunders, N. J., Hamoen, L. W. and Daniel, R. A. (2009) Two-step assembly dynamics of the *Bacillus subtilis* divisome. *J Bacteriol* **191**: 4186-4194.

Gorby, Y. A., Beveridge, T. J. and Blakemore, R. (1988) Characterization of the bacterial magnetosome membrane. *J Bacteriol* **170**: 834-841.

Grünberg, K., Müller, E. C., Otto, A., Reszka, R. and Linder, D. (2004) Biochemical and proteomic analysis of the magnetosome membrane in *Magnetospirillum gryphiswaldense*. *Appl Environ Microbiol* **70**: 1040-1050.

Grünberg, K., Wawer, C., Tebo, B. M. and Schüler, D. (2001) A large gene cluster encoding several magnetosome proteins is conserved in different species of magnetotactic bacteria. *Appl Environ Microbiol* **67**: 4573-4582.

Ho, S., Hunt, H., Horton, R., Pullen, J. and Pease, L. (1989) Site-directed mutagenesis by overlap extension using the polymerase chain reation. *Gene* **77**: 51-59.

Jogler, C., Kube, M., Schübbe, S., Ullrich, S., Teeling, H., Bazylinski, D. A., et al. (2009a) Comparative analysis of magnetosome gene clusters in magnetotactic

For Peer Review

bacteria provides further evidence for horizontal gene transfer. *Environ Microbiol* **11**: 1267-1277.

Jogler, C., Lin, W., Meyerdierks, A., Kube, M., Katzmann, E., Flies, C., et al. (2009b) Toward cloning of the magnetotactic metagenome: identification of magnetosome island gene clusters in uncultivated magnetotactic bacteria from different aquatic sediments. *Appl Environ Microbiol* **75**: 3972-3979.

Jogler, C. and Schüler, D. (2007) Genetic analysis of magnetosome biomineralization. In: Magnetoreception and magnetosomes in bacteria. D., S. (ed). Springer-Verlag Berlin Heidelberg, pp. 133-161.

Jogler, C. and Schüler, D. (2009) Genomics, genetics, and cell biology of magnetosome formation. *Annu Rev Microbiol* **63**: 501-521.

Jones, L. J., Carballido-Lopez, R. and Errington, J. (2001) Control of cell shape in bacteria: helical, actin-like filaments in *Bacillus subtilis*. *Cell* **104**: 913-922.

Katzen, F., Becker, A., Ielmini, M. V., Oddo, C. G. and Ielpi, L. (1999) New mobilizable vectors suitable for gene replacement in gram-negative bacteria and their use in mapping of the 3' end of the *Xanthomonas campestris* pv. *campestris* gum operon. *Appl Environ Microbiol* **65**: 278-282.

Kawaguchi, R., Burgess, J. and Matsunaga, T. (1992) Phylogeny and 16S rRNA sequence of *Magnetospirillum sp*. AMB-1, an aerobic magnetic bacterium. *Nucl Acids Res* **20**: 1140.

Kirschvink, J. L. (1982) Paleomagnetic evidence for fossil biogenic magnetite in western Crete. *Earth Plan Sci Lett* **59**: 388-392.

Kobayashi, A., Kirschvink, J. L., Nash, C. Z., Kopp, R. E., Sauer, D. A., Bertani, L. E., et al. (2006) Experimental observation of magnetosome chain collapse in

For Peer Review

magnetotactic bacteria: sedimentological, paleomagnetic, and evolutionary implications. *Earth Plan Sci Lett* **245**: 538-550.

Komeili, A. (2006) Cell biology of magnetosome formation. In: Magnetoreception and magnetosomes in bacteria. Schüler, D. (ed). Springer-Verlag Berlin Heidelberg, pp. 163-173.

Komeili, A. (2007) Molecular mechanisms of magnetosome formation. *Annu Rev Biochem* **76**: 351-366.

Komeili, A., Li, Z., Newman, D. K. and Jensen, G. J. (2006) Magnetosomes are cell membrane invaginations organized by the actin-like protein MamK. *Science* **311**: 242-245.

Komeili, A., Vali, H., Beveridge, T. J. and Newman, D. K. (2004) Magnetosome vesicles are present before magnetite formation, and MamA is required for their activation. *Proc Natl Acad Sci USA* **101**: 3839-3844.

Kovach, M. E., Phillips, R. W., Elzer, P. H., Roop, R. M. and Peterson, K. M. (1994) pBBR1MCS: a broad-host-range cloning vector. *BioTechniques* **16**: 800-802.

Laemmli, U. K. (1970) Cleavage of structural proteins during the assembly of the head of bacteriophage T4. *Nature* **227**: 680-685.

Lang, C., Pollithy, A. and Schüler, D. (2009) Identification of promoters for efficient gene expression in *Magnetospirillum gryphiswaldense*. *Appl Environ Microbiol* **75**: 4206-4210.

Li, J. L., Pan, Y., Chen, G., Liu, Q., Tian, L. and Lin, W. (2009) Magnetite magnetosome and fragmental chain formation of *Magnetospirillum magneticum* AMB-1: transmission electron microscopy and magnetic observations. *Geophys J Int* **177**: 33-42.

For Peer Review

Li, Z. and Jensen, G. (2009) Electron cryotomography: a new view into microbial ultrastructure. *Curr Opin Microbiol* **12**: 1-8.

Li, Z., Trimble, M. J., Brun, Y. V. and Jensen, G. (2007) The structure of FtsZ filaments in vivo suggests a force-generating role in cell division. *EMBO J* **26**: 4694-4708.

Lučić, V., Forster, F. and Baumeister, W. (2005) Structural studies by electron tomography: from cells to molecules. *Annual Reviews of Biochemistry* **74**: 833-865.

Marmur, J. (1961) A procedure for the isolation of deoxiribonucleic acid from microorganisms. *J Mol Biol* **3**: 208-218.

Mastronarde, D. N. (2005) Automated electron microscope tomography using robust prediction of specimen movements. *J Struct Biol* **152**: 36-51.

Milne, J. L. S. and Subramaniam, S. (2009) Cryo-electron tomography of bacteria: progress, challenges and future prospects. *Nat Rev Microbiol* **7**: 666-675.

Møller-Jensen, J., Jensen, R. B., Löwe, J. and Gerdes, K. (2002) Prokaryotic DNA segregation by an actin-like filament. *EMBO J* **21**: 3119-3127.

Murat, D., Quinlan, A., Vali, H. and Komeili, A. (2010) Comprehensive genetic dissection of the magnetosome gene island reveals the step-wise assembly of a prokaryotic organelle. *Proc Natl Acad Sci U S A* **107**: 5593-5598.

Nakazawa, H., Arakaki, A., Narita-Yamada, S., Yashiro, I., Jinno, K., Aoki, N., et al. (2009) Whole genome sequence of *Desulfovibrio magneticus* strain RS-1 revealed common gene clusters in magnetotactic bacteria. *Genome Res* **19**: 1801-1808.

For Peer Review

Nickell, S., Forster, F., Linaroudis, A., Net, W. D., Beck, F., Hegerl, R., et al. (2005) TOM software toolbox: acquisition and analysis for electron tomography. *J Struct Biol* **149**: 227-234.

Ohuchi, S. and Schüler, D. (2009) *In vivo* display of a multisubunit enzyme complex on biogenic magnetic nanoparticles. *Appl Environ Microbiol* **75**: 7734-7738.

Pradel, N., Santini, C., Bernadac, A., Fukumori, Y. and Wu, L. (2006) Biogenesis of actin-like bacterial cytoskeletal filaments destined for positioning prokaryotic magnetic organelles. *Proc Natl Acad Sci USA* **103**: 17485-17489.

Pradel, N., Santini, C., Bernadac, A., Shih, Y., Goldberg, M. and Wu, L. (2007) Polar positional information in *Escherichia coli* spherical cells. *Biochem Bioph Res Co* **353**: 493-500.

Richter, M., Kube, M., Bazylinski, D. A., Lombardot, T., Glöckner, F. O., Reinhardt, R. and Schüler, D. (2007) Comparative genome analysis of four magnetotactic bacteria reveals a complex set of group-specific genes implicated in magnetosome biomineralization and function. *J Bacteriol* **189**: 4899-4910.

Rioux, J.-B., Philippe, N., Pereira, S., Pignol, D., Wu, L.-F. and Ginet, N. (2010) A second actin-like MamK protein in *Magnetospirillum magneticum* AMB-1 encoded outside the genomic magnetosome island. *PLoS ONE* **5**: e9151.

Salje, J. and Löwe, J. (2008) Bacterial actin: architecture of the ParMRC plasmid DNA partitioning complex. *EMBO J* **27**: 2230-2238.

Sambrook, J. and Russel, D. (2001) *Molecular cloning: a laboratory manual.,* p. 999. Cold Spring Harbor Laboratory Press.

For Peer Review

Scheffel, A. (2007) Molekulare und strukturelle Untersuchung zur Bildung von Magnetosomen und zur Assemblierung von Magnetosomenketten. *Doctoral thesis*. 1-194.

Scheffel, A., Gruska, M., Faivre, D., Linaroudis, A., Graumann, P. L., Plitzko, J. and Schüler, D. (2006) An acidic protein aligns magnetosomes along a filamentous structure in magnetotactic bacteria. *Nature* **440**: 110-114.

Scheffel, A. and Schüler, D. (2007) The acidic repetitive domain of the *Magnetospirillum gryphiswaldense* MamJ protein displays hypervariability but is not required for magnetosome chain assembly. *J Bacteriol* **189**: 6437-6446.

Schübbe, S. (2005) Untersuchung zur molekularen Regulation und Organisation der *mam*-Gene in *Magnetospirillum gryphiswaldense* MSR-1. *Doctoral thesis*. 1-167.

Schübbe, S., Kube, M., Scheffel, A., Wawer, C., Heyen, U., Meyerdierks, A., et al. (2003) Characterization of a spontaneous nonmagnetic mutant of *Magnetospirillum gryphiswaldense* reveals a large deletion comprising a putative magnetosome island. *J Bacteriol* **185**: 5779-5790.

Schübbe, S., Würdemann, C., Peplies, J., Heyen, U., Wawer, C., Glöckner, F. O. and Schüler, D. (2006) Transcriptional organization and regulation of magnetosome operons in *Magnetospirillum gryphiswaldense*. *Appl Environ Microbiol* **72**: 5757-5765.

Schüler, D. (2004a) Characterization of the magnetosome membrane in *Magnetospirillum gryphiswaldense*. In: Biominerlization. Baeuerlein, E. (ed). Wiley-VCH Verlag GmbH, pp. 109-118.

For Peer Review

Schüler, D. (2004b) Molecular analysis of a subcellular compartment: The magnetosome membrane in *Magnetospirillum gryphiswaldense*. *Arch Microbiol* **181**: 1-7.

Schüler, D. (2008) Genetics and cell biology of magnetosome formation in magnetotactic bacteria. *FEMS Microbiol Rev* **32**: 654-672.

Schüler, D. and Köhler, M. (1992) The isolation of a new magnetic spirillum. *Zentralbl Mikrobiol* **147**: 150-151.

Schultheiss, D., Kube, M. and Schüler, D. (2004) Inactivation of the flagellin gene *flaA* in *Magnetospirillum gryphiswaldense* results in nonmagnetotactic mutants lacking flagellar filaments. *Appl Environ Microbiol* **70**: 3624-3631.

Schultheiss, D. and Schüler, D. (2003) Development of a genetic system for *Magnetospirillum gryphiswaldense*. *Arch Microbiol* **179**: 89-94.

Simpson, E. T. (2008) Electron holography of isolated and interacting magnetic nanocrystals. *Doctoral thesis*. 1-197.

Taoka, A., Asada, R., Sasaki, H., Anzawa, K., Wu, L. and Fukumori, Y. (2006) Spatial localizations of Mam22 and Mam12 in the magnetosomes of *Magnetospirillum magnetotacticum*. *J Bacteriol* **188**: 3805-3812.

Taoka, A., Asada, R., Wu, L. and Fukumori, Y. (2007) Polymerization of the actin-like protein MamK, which is associated with magnetosomes. *J Bacteriol* **189**: 8737-8740.

Ullrich, S., Kube, M., Schübbe, S., Reinhardt, R. and Schüler, D. (2005) A hypervariable 130-kilobase genomic region of *Magnetospirillum gryphiswaldense* comprises a magnetosome island which undergoes frequent rearrangements during stationary growth. *J Bacteriol* **187**: 7176-7184.

For Peer Review

Vats, P., Shih, Y.-L. and Rothfield, L. (2009) Assembly of the MreB-associated cytoskeletal ring of *Escherichia coli*. *Mol Microbiol* **72**: 170-182.

For Peer Review

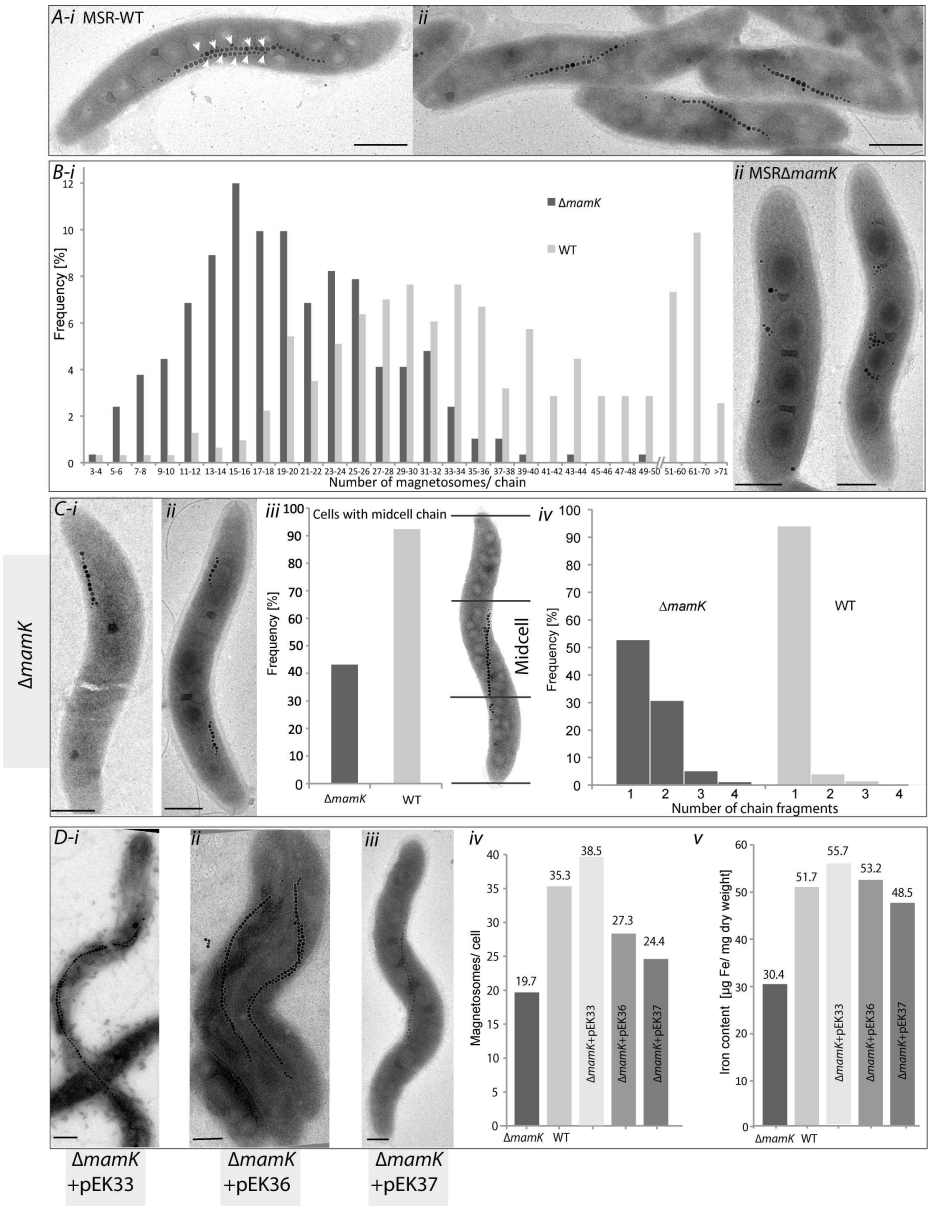


Fig. 1: Overview of morphologies and magnetosome chain organizations found in MSRΔ*mamK* cells and WT. (A*i*-*ii*) TEM micrographs of MSR WT cells. White arrows indicate parallel chains. (B*i*) Statistical analysis of magnetosome particles per chain and micrographs of MSRΔ*mamK* cells displaying dispersed magnetosomes (B*ii*). (C*i*-*ii*) Micrographs of MSRΔ*mamK* cells displaying ectopic chain localization, and statistical analysis of chain position (*iii*), and chain numbers (*iv*) in MSRΔ*mamK*. (D*i*-*iii*) TEM micrographs of transcomplemented MSRΔ*mamK* cells with various plasmids. Magnetosome numbers and iron contents of the strains are shown in (D*v*-*vi*). Scale bars 500 nm.

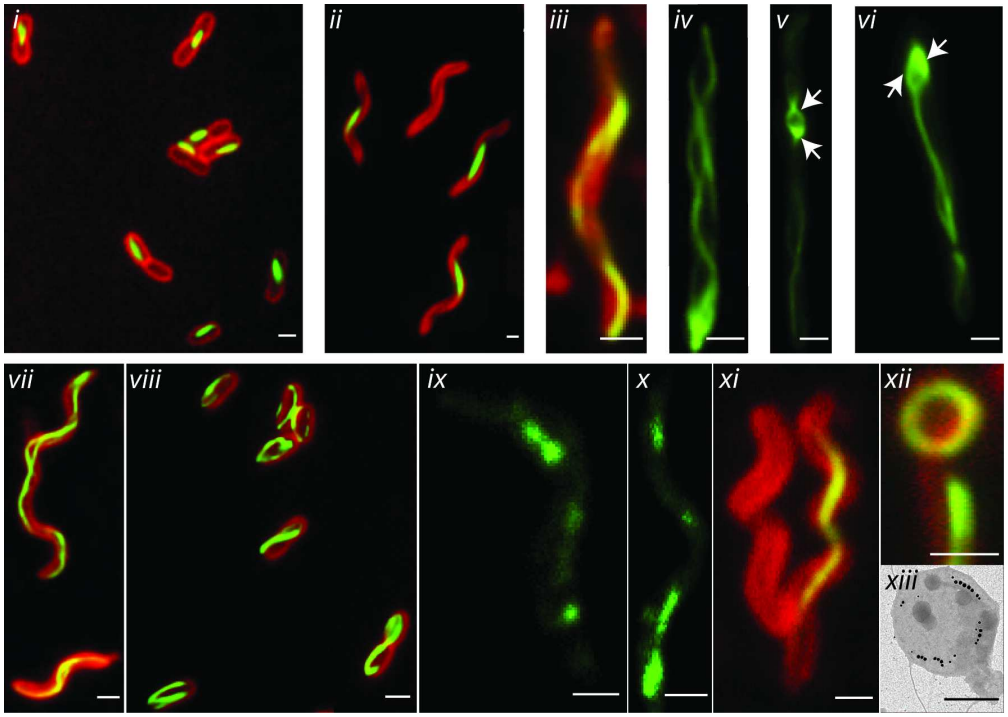


Fig. 2: Fluorescence micrographs of *E. coli*, MSR ( and MSR-1B) and AMB expressing different EGFP fusions. (*i*) Overlay of FM4-64 (red) and *egfp* (green) recombinant *E.coli* expressing pAS_K1. Localization pattern of MamK_GSI_eGFP. (*ii*) pAS_K1 expressed in non-magnetic mutant MSR-1B. (*iii*) MSR WT expressing pAS_K. (*iv* - *vi*) MSRΔ*mamK* mutant of MSR-1 expressing pAS_K (eGFP_LCLQGE_MamK) resulting in loop-shaped or spiral localization patterns. Loop-like structures are observed at midcell (white arrows). (*vii*) pAS_K expressed in MSR-1B exhibiting helical filaments. (*viii*) Overlay of FM4-64 and *egfp* image of recombinant *E. coli* expressing pAS_K. Helical filaments are visible. (*ix* - *x*) MSRΔmamK mutant expressing eGFP fused MamJ (pAS_J). (*xi*) Overlay of FM4-64 and *egfp* of AMB WT expressing pAS_K resulting in a long filamentous localization throughout the entire cell. (*xii*) MSRΔ*mamK* mutant expressing pAS_K in MSRΔ*mamK* in a spheroplast cell. (*xiii*) TEM micrograph of a spheroplast cell. Scale bars 500 nm.
150x106mm (300 x 300 DPI)

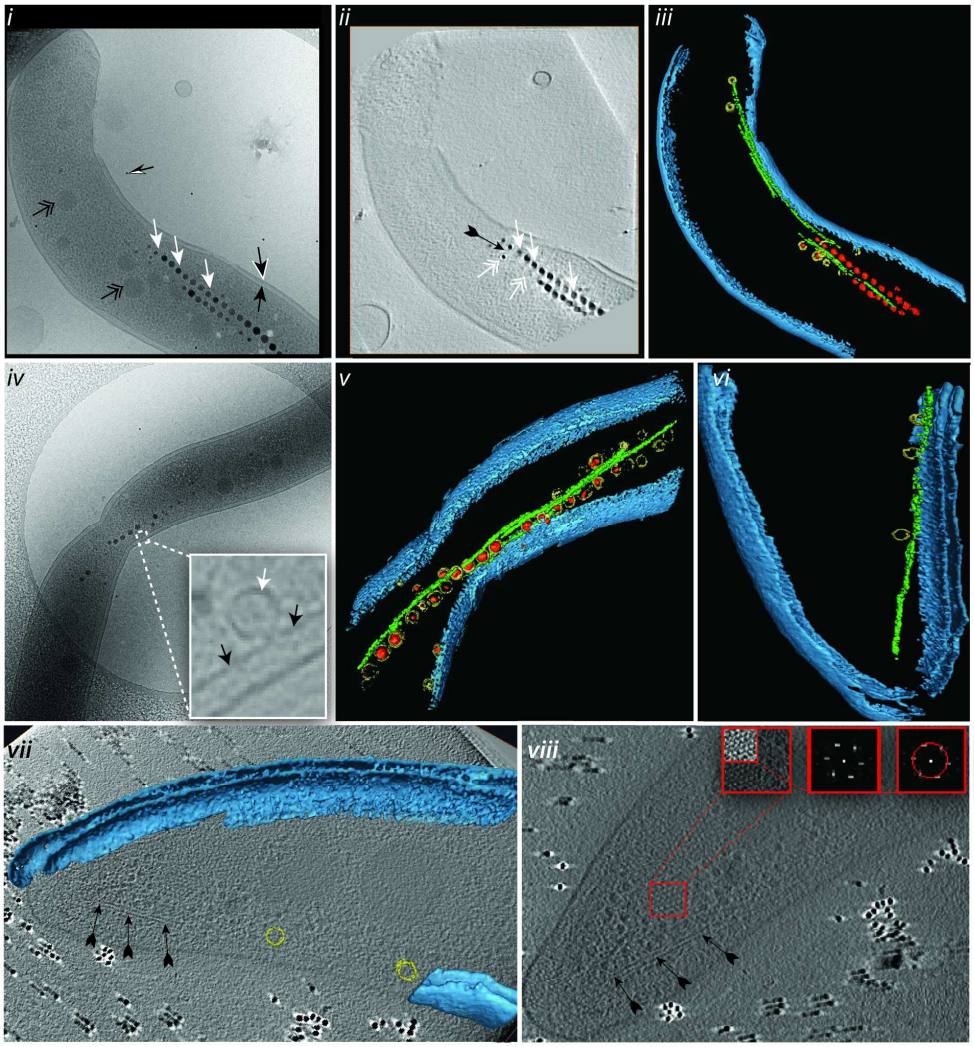


Fig. 3: Cryo-electron micrographs and tomograms of MSR WT. (*i*) Cryo-electron micrograph of a WT cell after the acquisition of a tilt series in vitrified ice. (*ii*) x-y slice of a tomogram from (*i*). (*iii*) Surface rendered volume the WT cell. Depicted are the cell membrane (blue), magnetite crystals (red), vesicles (yellow) and filaments (green). (*iv*) Cryo-electron micrograph of WT cell in early division state after acquisition of a tilt series. Inset *iv*: MM vesicle from *iv* invaginating from the CM (black arrows CM, white arrow MM). (*v*) Surface rendered volume of cell shown in (*iv*). (*vi*) Surface rendered pole of MSR WT cell exhibiting filaments close to the pole membrane. (*vii*-*viii*) x-y slices of WT tomogram (*vi*). (Insets of *viii*): power spectra of a putative chemoreceptor array, lattice distance 10.5 nm. Arrow tips; black: CM and black with white rim OM, black-white: fiducial gold marker (15nm), white: magnetite crystals, double-white (*ii*): vesicle membrane, black with fletching: filament, double-black: PHB granules.
165x172mm (300 x 300 DPI)

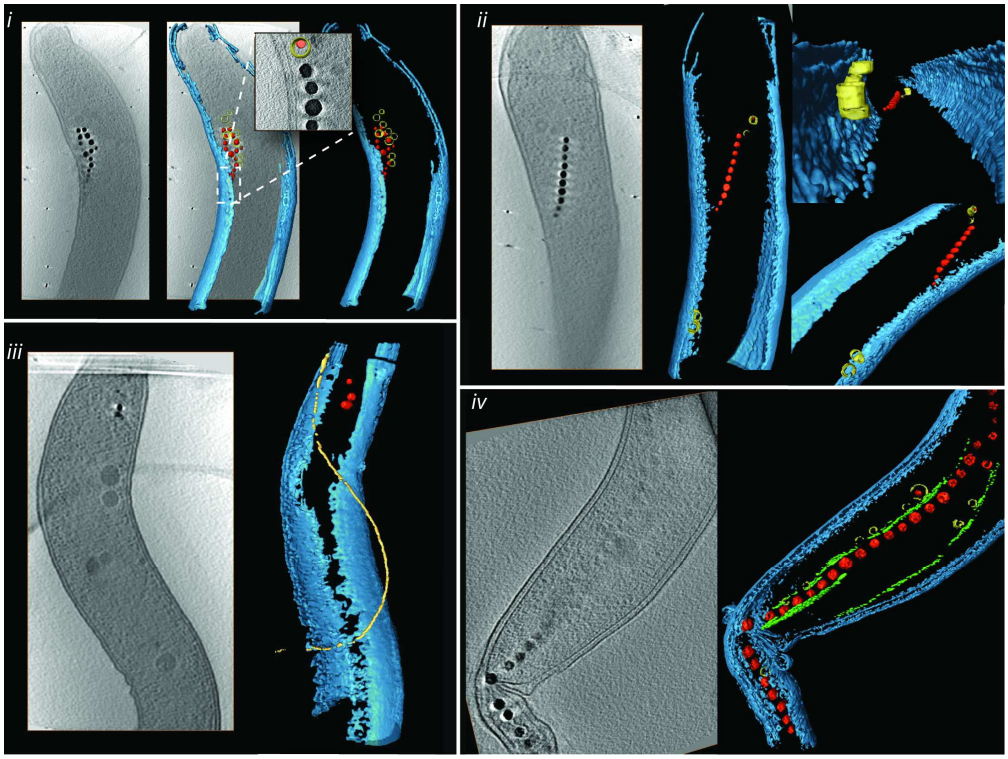


Fig. 4: (*i-iv*) Cryo-electron tomograms of MSRΔ*mamK* in early stationary phase grown under standard conditions (30°C, FSM medium), flagella (yellow) in (*iii*). (*iv*) transcomplemented MSRΔ*mamK* mutant in late division state expressing mamK from pEK42. Surface-rendered representation of a segment of the cells showing vesicles (yellow) and magnetite crystals (red). Different three-dimensional orientations show the variety of the pleiotropic phenotypes (membrane in blue) of MSRΔ*mamK* mutants. The apparent absence of MM (vesicles, yellow) from mature magnetite crystals (red) is due to the adverse effect of variable diffraction contrast during tilting as a result of the crystalline magnetite.
184x138mm (300 x 300 DPI)

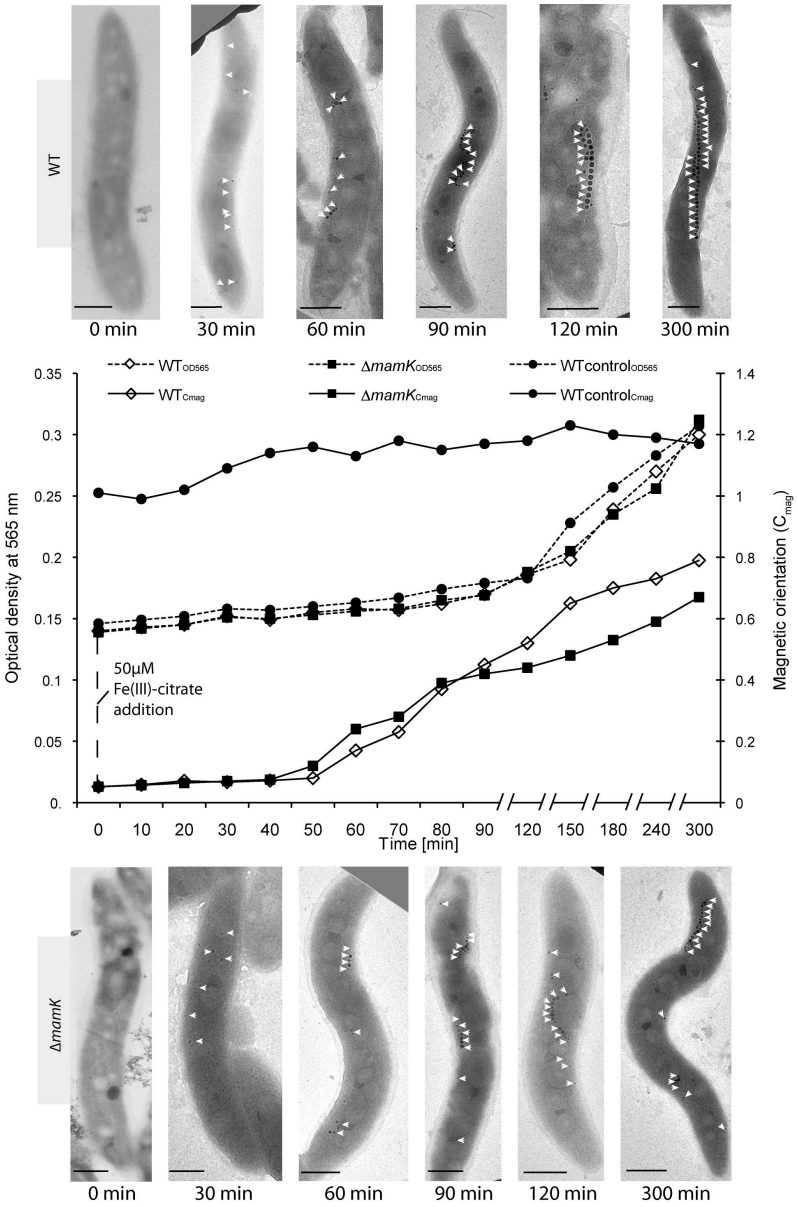


Fig. 5: Time course of magnetosome synthesis and chain assembly after iron induction in *M. gryphiswaldense* WT and MSRΔ*mamK*. Non-magnetic cells were cultured for 300 min in LIM. 50 µM Fe(III)-citrate was added at 0 min and growth (dashed line) was analyzed by optical density at 565 nm. WTcontrol cells were cultured under standard un-induced growth conditions in 50 µM Fe(III)-citrate FSM medium. Solid lines: magnetic orientation (Cmag). Electron micrographs of cells from aliquots taken at various time points are shown. Scale bars 500 nm.